ISSN 1392-1207. MECHANIKA. Vol. 31, No. 1, 2025: 35–43

Study on Simultaneous Identification of External Excitation and Response Reconstruction for Continuous System

Hongqiu LI*, Jinhui JIANG, M Shadi MOHAMED*****

**Mechatronic Engineering College, Jinling Institute of Technology, Nanjing 211169, China, E-mail: lihongqiu@jit.edu.cn*
***State Key Laboratory of Mechanics and Control for Aerospace structures, Nanjing University of Aeronautics and Astronautics, Nanjing 210016, China, E-mail: jiangjinhui@nuaa.edu.cn (Corresponding Author)*
****Institute for Infrastructure and Environment, Heriot-Watt University, Edinburgh EH14 4AS, UK, E-mail: M.S.Mohamed@hw.ac.uk*

https://doi.org/10.5755/j02.mech.38958

1. Introduction

In aerospace, mechanical, and civil engineering, structural vibrations pose significant hazards. Dynamic loads can greatly affect the safety and stability of structures [1]. Obtaining dynamic load data, especially from hard-to-measure and critical points, is essential for research and structural health monitoring [2].

Structural dynamic response reconstruction (DRR) technology can extrapolate abundant data from a limited number of measurement points, partially compensating for insufficient measurement data. Therefore, an algorithm capable of simultaneously identifying structural dynamic loads and reconstructing responses is vital.

Response reconstruction on precise structural models is a traditional problem. However, the structural parameters of actual engineering structures are unknown. It is essential to investigate the issue of dynamic load identification for uncertain structures [3]. Jiang et al. [4] proposed a novel dynamic load identification method that takes into account unknown initial conditions of structures which is based on the improved basis functions and implicit Newmark-β method. Cui et al. [5] introduced a convolutional neural network (CNN) for the reconstruction of the interval of unknown load. Combining the interval analysis theory with Taylor expansion, the upper and lower boundaries of the supervised loads are obtained and used as training samples. The trained CNN model can directly identify the boundaries of the unknown load interval. Yang et al. [6] proposed a novel method based on a deep dilated convolution neural network (DCNN) for dynamic load identification, directly constructing the inverse model between vibration response and excitation, avoiding solving the model parameter. The method for reconstructing dynamic responses in uncertain structures within linear systems relies on Kalman filtering. While classical Kalman filtering addresses uncertain models, obtaining specific excitation information is necessary. Li et al. [7] proposed a method allows for identifying earthquake ground motion using incomplete modal information and limited measurements through the standard Kalman filter. Naets et al. [8] utilized an improved augmented Kalman filter algorithm based on measurement to resolve prediction result divergence. Aucejo et al. [9] explored the adaptability of the adaptive Kalman filter (AKF) in reconstructing mechanical sources, proposing a new state space representation of dynamic systems based on a generalized method. Under the augmented Kalman filter, using only the accelerometer signal may result in algorithm recognition divergence due to the unobservability and insufficient rank of the augmented matrix. Maes et al. [10] proposed a Joint Input State Estimation (JISE) algorithm that considers the correlation between model and measurement errors to quantify estimation uncertainty caused by measurement errors and unknown random excitations.

Huang et al. [11] proposed two generalized algorithms based on generalized Kalman filtering under unknown input (GKF-UI) for the identification of seismic ground excitation to multi-story and tall buildings, respectively. Álvarez-Briceño et al. [12] used state-augmented Kalman filter (AKF) algorithm to estimate a point random force, which is applied at the end of a cantilevered structure. Hassanabadi et al. [13] proposed a linear recursive Bayesian filter for minimum variance unbiased joint input and state estimation of structural systems, in which unknown inputs are estimated without attributing any fictitious input model or statistics.

The Kalman filtering algorithm shows promise in reconstructing structural dynamic responses, particularly in cases with model errors. However, simultaneous reconstruction of structural external excitation and response has received limited attention [14]. In this paper, we propose an excitation prediction Kalman filtering algorithm for reconstructing structural dynamic responses, based on the classical Kalman filtering method for continuous system.

Initially, we derived the load identification theory of continuous system by taking the simply supported beam as an example in modal space. Then, using the same continuous system as a simulation example, we analyse the accuracy of the response signal identified and reconstructed by our algorithm under a fixed frequency external excitation. Additionally, we introduce various noise conditions and model errors to assess the algorithm's robustness against noise. Finally, we validate the feasibility and reliability of both the system and the structural DRR algorithm through experiments.

2. Structural DRR algorithm based on Bayesian method for continuous system

2.1. Simply supported beam model and equation of motion in modal space

This paper derives the load identification theory of continuous system by taking the simply supported beam as an example. The model of the simply supported beam is shown in Fig. 1.

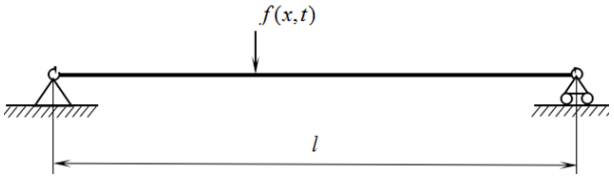

Fig. 1 Simply supported beam model under concentrated force

It is assumed that the beam shown in the Fig. 1 is a homogeneous Bernoulli-Euler beam [15] with equal sections. The differential equation of bending vibration of the beam can be obtained as

$$\rho A\frac{\partial^2 w(x,t)}{\partial t^2}+EI\frac{\partial^4 w(x,t)}{\partial x^4}+ +CEI\frac{\partial^5 w(x,t)}{\partial t\partial x^4}=f(x,t), \tag{1}$$

here, A is the cross-sectional area, and C, E and ρ represent the damping coefficient, the elastic modulus of the material and the material density, respectively. I represents the moment of inertia of the section about the neutral axis. The lateral external force distributed on the beam per unit length is denoted by $f(x,t)$; $w(x,t)$ represents the transverse displacement of the cross-section neutral axis with coordinates x at time t.

The partial differential equation of the continuous system can be transformed into a series of ordinary differential equations represented by the main coordinate. Introducing the principal coordinate transformation by using the modal superposition method:

$$w(x,t)=\sum_{n=1}^{+\infty}W_n(x)q_n(t)\ , \tag{2}$$

where $W_n(x)$ represents the n-th mode shape function, and $q_n(t)$ is a time function describing the motion law. It is assumed that the mode shapes of the system have been normalized with respect to the mass. The orthogonality of mode shape function can be expressed as:

$$\begin{cases}\int_0^l \rho A W_n(x)W_m(x)dx=\delta_{nm}\\ \int_0^l EIW_n''(x)W_m''(x)dx=\omega_n^2\delta_{nm}\end{cases},$$

$n, m = 1, 2, 3...,$ (3)

where ω_n is the nth order modal frequency, and

$$\delta_{nm}=\begin{cases}1, & n=m\\ 0, & n\neq m\end{cases}. \tag{4}$$

According to the orthogonality of mode shape function, Eq. (5) can be obtained by multiplying $W_n(x)$ by both sides of Eq. (1) and integrating x along the length of the beam:

$$\ddot{q}_n(t)+2\xi_n\omega_n\dot{q}_n(t)+\omega_n^2 q_n(t)=f_n(t),$$

$n = 1, 2, 3...$ (5)

where ξ_n and $f_n(t)$ are the n-th order modal damping ratio and modal force, respectively. High order modes contribute little to the vibration response of the system, hence, the modal truncation method can be used to reduce the DoF of the system. It is assumed that the modal truncation order is r, and Eq. (5) can be transformed into a finite number of independent equations as:

$$\ddot{\boldsymbol{q}}(t)+\boldsymbol{\Lambda}\dot{\boldsymbol{q}}(t)+\boldsymbol{\Gamma}\boldsymbol{q}(t)=\boldsymbol{f}^r(t), \tag{6}$$

where

$$\ddot{\boldsymbol{q}}(t)=\begin{Bmatrix}\ddot{q}_1(t)\\ \ddot{q}_2(t)\\ \vdots\\ \ddot{q}_r(t)\end{Bmatrix},\quad \dot{\boldsymbol{q}}(t)=\begin{Bmatrix}\dot{q}_1(t)\\ \dot{q}_2(t)\\ \vdots\\ \dot{q}_r(t)\end{Bmatrix},\quad \boldsymbol{q}(t)=\begin{Bmatrix}q_1(t)\\ q_2(t)\\ \vdots\\ q_r(t)\end{Bmatrix},$$

$$\boldsymbol{f}^r(t)=\begin{Bmatrix}f_1(t)\\ f_2(t)\\ \vdots\\ f_r(t)\end{Bmatrix},\quad \boldsymbol{\Lambda}=\begin{bmatrix}2\xi_1\omega_1 & 0 & \cdots & 0\\ 0 & 2\xi_2\omega_2 & \cdots & 0\\ \vdots & \vdots & \ddots & \vdots\\ 0 & 0 & \cdots & 2\xi_r\omega_r\end{bmatrix},$$

$$\boldsymbol{\Gamma}=\begin{bmatrix}\omega_1^2 & 0 & \cdots & 0\\ 0 & \omega_2^2 & \cdots & 0\\ \vdots & \vdots & \ddots & \vdots\\ 0 & 0 & \cdots & \omega_r^2\end{bmatrix}.$$

To transform the dynamic motion Eq. (6) into a linear state-space form we can write:

$$\dot{\boldsymbol{x}}(t)=\boldsymbol{A}_c\boldsymbol{x}(t)+\boldsymbol{B}_c\boldsymbol{u}(t), \tag{7}$$

$$\boldsymbol{y}(t)=\boldsymbol{H}\boldsymbol{x}(t)+\boldsymbol{D}\boldsymbol{u}(t), \tag{8}$$

where

$$\boldsymbol{x}(t)=\begin{bmatrix}\boldsymbol{q}(t)\\ \dot{\boldsymbol{q}}(t)\end{bmatrix},\ \boldsymbol{A}_c=\begin{bmatrix}\boldsymbol{0} & \boldsymbol{I}\\ -\boldsymbol{\Lambda} & -\boldsymbol{\Gamma}\end{bmatrix},\ \boldsymbol{B}_c=\begin{bmatrix}\boldsymbol{0}\\ \boldsymbol{I}\end{bmatrix},$$

$$\boldsymbol{u}(t)=\boldsymbol{f}^r(t) \tag{9}$$

The vector $\boldsymbol{x}(t)$, $\boldsymbol{y}(t)$ are the structure state vector and measurement vector respectively, while $\boldsymbol{A}_c$ is the state transfer matrix. $\boldsymbol{B}_c$ is the influence matrix of external excitation, which consists of 0 and 1. The location of the excitation is 1, and the rest of the positions are 0. $\boldsymbol{H}$ and $\boldsymbol{D}$ being the observation matrix and excitation influence matrix respectively.

Assuming equispaced sampling time instants i.e. $t(t = t_0, t_1, t_2, \ldots, t_k, \ldots)$ and assuming these instants are small enough, we can also reasonably assume that the excitation $\boldsymbol{u}(t)$ remains unchanged within ($\Delta t = t_{k+1}-t_k$), and the Eqs. (7) and (8) can be discretized as:

$$\begin{aligned}\boldsymbol{x}_{k+1}&=\boldsymbol{A}\boldsymbol{x}_k+\boldsymbol{B}\boldsymbol{u}_k\\ \boldsymbol{y}_k&=\boldsymbol{H}\boldsymbol{x}_k+\boldsymbol{D}\boldsymbol{u}_k\end{aligned}, \tag{10}$$

where $\boldsymbol{u}_k$ is the external excitation, $\boldsymbol{x}_{k+1}$ and $\boldsymbol{x}_k$ represent the structural state vectors at time $(k + 1)\Delta t$ and $k\Delta t$,

respectively. Here, $\boldsymbol{A}$ and $\boldsymbol{B}$ are the state transition matrix and the excitation influence matrix in a discrete format and defined as:

$$\boldsymbol{A} = \mathrm{e}^{\boldsymbol{A}_c \Delta t} \ , \tag{11}$$

$$\boldsymbol{B} = \int_0^{\Delta t} \boldsymbol{A}(0,\tau)\boldsymbol{B}_c \mathrm{d}\tau = \int_0^{\Delta t} \mathrm{e}^{\boldsymbol{A}_c \tau}\boldsymbol{B}_c \mathrm{d}\tau = \\ = \int_0^{\Delta t} \mathrm{e}^{\boldsymbol{A}_c \tau}\mathrm{d}\tau \boldsymbol{B}_c = \left(\boldsymbol{A} - \boldsymbol{I}\right)\boldsymbol{A}_c^{-1}\boldsymbol{B}_c. \tag{12}$$

This paper proposes a structural DRR method based on the excitation prediction Kalman filter, which includes an excitation identification step and uses weighted least squares to identify the excitation. Combining Kalman filtering for state estimation, utilizing time update steps and measurement update steps to achieve recursion and state correction, can simultaneously achieve excitation recognition and response reconstruction.

The specific calculation process is as follows.

1. Time update step

According Eq. (10), we obtain

$$\boldsymbol{x}_{k|k-1} = \boldsymbol{A}\boldsymbol{x}_{k-1|k-1} + \boldsymbol{B}\hat{\boldsymbol{u}}_{k-1}, \tag{13}$$

where $\mathbf{x}_{k|k-1}$ is a priori estimate, $\mathbf{x}_{k-1|k-1}$ is a posteriori estimate of time k–1.

The error of the estimate of $\mathbf{x}_{k|k-1}$ is

$$\tilde{\boldsymbol{x}}_{k|k-1} \equiv \boldsymbol{x}_k - \boldsymbol{x}_{k|k-1} = \boldsymbol{A}\tilde{\boldsymbol{x}}_{k-1|k-1} + \boldsymbol{B}\tilde{\boldsymbol{u}}_{k-1} + w_{k-1}, \tag{14}$$

where, $\tilde{\mathbf{x}}_{k|k} \equiv \mathbf{x}_k - \mathbf{x}_{k|k}$, w_{k-1} is considered to be independent identically distributed Gaussian noise with the mean value 0.

2. Excitation identification step

Define residuals,

$$\tilde{\boldsymbol{y}}_k \equiv \boldsymbol{y}_k - \boldsymbol{H}\boldsymbol{x}_{k|k-1}, \tag{15}$$

with $\boldsymbol{y}_k = \boldsymbol{H}\boldsymbol{x}_k + \boldsymbol{D}\boldsymbol{u}_k + v_k$. (16)

Get the relationship between $\tilde{\boldsymbol{y}}_k$ and $\boldsymbol{u}_k$

$$\tilde{\boldsymbol{y}}_k = \boldsymbol{D}\boldsymbol{u}_k + \boldsymbol{H}\tilde{\boldsymbol{x}}_{k|k-1} + v_k = \boldsymbol{D}\boldsymbol{u}_k + \boldsymbol{e}_k , \tag{17}$$

where $\boldsymbol{e}_k = \boldsymbol{H}\tilde{\boldsymbol{x}}_{k|k-1} + v_k$. Since $\boldsymbol{x}_{k|k-1}$ is an unbiased estimation and $E(v_k) = 0$, $E(\boldsymbol{e}_k) = 0$; we can write $E\left(\tilde{\boldsymbol{y}}_k\right) = \boldsymbol{D}E\left(\boldsymbol{u}_k\right)$. Next, the external excitation is estimated as:

$$\hat{\boldsymbol{u}}_k = \boldsymbol{J}_k\left(\boldsymbol{y}_k - \boldsymbol{H}\boldsymbol{x}_{k|k-1}\right), \tag{18}$$

where $\boldsymbol{J}_k$ is to be solved parameter, which makes $\hat{\boldsymbol{u}}_k$ be unbiased estimation of the external excitation $\boldsymbol{u}_k$

Replacing Eq. (18) with Eq. (16), we obtain

$$\hat{\boldsymbol{u}}_k = \boldsymbol{J}_k\boldsymbol{D}\boldsymbol{u}_k + \boldsymbol{J}_k\boldsymbol{e}_k . \tag{19}$$

If $\hat{\boldsymbol{u}}_k$ is an unbiased estimate of $\boldsymbol{u}_k$, then $\boldsymbol{J}_k\boldsymbol{D} = \boldsymbol{I}$. Let

$$\tilde{\boldsymbol{R}}_k \equiv E\left(\boldsymbol{e}_k\boldsymbol{e}_k^T\right) = \boldsymbol{H}\boldsymbol{P}_{k|k-1}^x\boldsymbol{H}^T + \boldsymbol{R}_k . \tag{20}$$

In the above formula $\boldsymbol{R}_k \equiv E\left(v_k v_k^T\right)$, $\tilde{\boldsymbol{R}}_k$ is a positive definite matrix. According to the least squares method, it can be inferred that:

$$\boldsymbol{J}_k = \left(\boldsymbol{D}^T\tilde{\boldsymbol{R}}_k^{-1}\boldsymbol{D}\right)^{-1}\boldsymbol{D}^T\tilde{\boldsymbol{R}}_k^{-1} . \tag{21}$$

Predicting $\boldsymbol{u}_k$ is also a parameter estimation method similar to weighted least squares. Let $\tilde{\boldsymbol{y}}_k$ be the observation value and the $\tilde{\boldsymbol{R}}_k^{-1}$ be the weight, then the variance $\boldsymbol{P}_k^u$ of $\tilde{\boldsymbol{u}}_k$ is

$$\boldsymbol{P}_k^u = E(\tilde{\boldsymbol{u}}_k\tilde{\boldsymbol{u}}_k^T) = \boldsymbol{J}_k\boldsymbol{e}_k\boldsymbol{e}_k^T\boldsymbol{J}_k^T = \boldsymbol{J}_k\left(\boldsymbol{H}\tilde{\boldsymbol{x}}_{k|k-1} + v_k\right)\left(\boldsymbol{H}\tilde{\boldsymbol{x}}_{k|k-1} + v_k\right)^T\boldsymbol{J}_k^T = \boldsymbol{J}_k\left(\boldsymbol{H}\boldsymbol{P}_{k|k-1}^x\boldsymbol{H}^T + \boldsymbol{R}_k\right)\boldsymbol{J}_k = \\ = \left(\boldsymbol{D}^T\tilde{\boldsymbol{R}}_k^{-1}\boldsymbol{D}\right)^{-1}\boldsymbol{D}^T\tilde{\boldsymbol{R}}_k^{-1}\tilde{\boldsymbol{R}}_k\tilde{\boldsymbol{R}}_k^{-1}\boldsymbol{D}\left[\left(\boldsymbol{D}^T\tilde{\boldsymbol{R}}_k^{-1}\boldsymbol{D}\right)^{-1}\right]^T = \left(\boldsymbol{D}^T\tilde{\boldsymbol{R}}_k^{-1}\boldsymbol{D}\right)^{-1} . \tag{22}$$

3. Measurement update step

For measurement update, we assume that,

$$\boldsymbol{x}_{k|k} = \boldsymbol{x}_{k|k-1} + \boldsymbol{K}_k\left(\boldsymbol{y}_k - \boldsymbol{H}\boldsymbol{x}_{k|k-1} - \boldsymbol{D}\hat{\boldsymbol{u}}_k\right), \tag{23}$$

where $\boldsymbol{K}_k$ is Kalman gain, which can be solved by minimizing the variance matrix using the weighted least squares method [16]

$$\boldsymbol{K}_k = \boldsymbol{P}_{k|k-1}^x\boldsymbol{H}^T\tilde{\boldsymbol{R}}_k^{-1}, \tag{24}$$

$$\boldsymbol{P}_{k|k}^x = \boldsymbol{P}_{k|k-1}^x - \boldsymbol{K}_k\left(\tilde{\boldsymbol{R}}_k^{-1} - \boldsymbol{D}\boldsymbol{P}_k^u\boldsymbol{D}^T\right)\boldsymbol{K}_k^T . \tag{25}$$

So far, the derivation of the Kalman filter algorithm based on excitation prediction has been completed. The time update step, force identification step, and measurement update step are detailed below:

$$\begin{aligned} &\boldsymbol{x}_{k|k-1} = \boldsymbol{A}\boldsymbol{x}_{k-1|k-1} + \boldsymbol{B}\hat{\boldsymbol{u}}_{k-1}, \\ &\hat{\boldsymbol{u}}_k = \boldsymbol{J}_k\left(\boldsymbol{y}_k - \boldsymbol{H}\boldsymbol{x}_{k|k-1}\right), \\ &\boldsymbol{x}_{k|k} = \boldsymbol{x}_{k|k-1} + \boldsymbol{K}_k\left(\boldsymbol{y}_k - \boldsymbol{H}\boldsymbol{x}_{k|k-1} - \boldsymbol{D}\hat{\boldsymbol{u}}_k\right). \end{aligned} \tag{26}$$

To sum up, the flow of Kalman filter algorithm based on excitation prediction is given in Table 1.

2.2. Structural DRR method

To achieve structural response reconstruction, which involves predicting the response value at a target point using signals from limited observation points, we

Table 1
Kalman filter algorithm based on excitation prediction

1.Given the initial value $\boldsymbol{x}_{0\|-1}$, $\boldsymbol{P}_{0\|-1}^{x}$.
2.Exciation identification step $\tilde{\boldsymbol{R}}_k = \boldsymbol{H}\boldsymbol{P}_{k\|k-1}^{x}\boldsymbol{H}^T + \boldsymbol{R}_k$, $\boldsymbol{J}_k = \left(\boldsymbol{D}^T\tilde{\boldsymbol{R}}_k^{-1}\boldsymbol{D}\right)^{-1}\boldsymbol{D}^T\tilde{\boldsymbol{R}}_k^{-1}$, $\hat{\boldsymbol{u}}_k = \boldsymbol{J}_k\left(\boldsymbol{y}_k - \boldsymbol{H}\boldsymbol{x}_{k\|k-1}\right)$, $\boldsymbol{P}_k^{u} = \left(\boldsymbol{D}^T\tilde{\boldsymbol{R}}_k^{-1}\boldsymbol{D}\right)^{-1}$.
3.Measurement update step $\boldsymbol{K}_k = \boldsymbol{P}_{k\|k-1}^{x}\boldsymbol{H}^T\tilde{\boldsymbol{R}}_k^{-1}$, $\boldsymbol{x}_{k\|k} = \boldsymbol{x}_{k\|k-1} + \boldsymbol{K}_k(\boldsymbol{y}_k - \boldsymbol{H}\boldsymbol{x}_{k\|k-1} - \boldsymbol{D}\hat{\boldsymbol{u}}_k)$, $\mathbf{P}_{k\|k}^{x} = \mathbf{P}_{k\|k-1}^{x} - \mathbf{K}_k(\tilde{\mathbf{R}}_k^{-1} - \mathbf{D}\mathbf{P}_k^{u}\mathbf{D}^T)\mathbf{K}_k^T$, $\boldsymbol{P}_k^{xu} = \left(\boldsymbol{P}_k^{ux}\right)^T = -\frac{n!}{r!(n-r)!_k}\boldsymbol{D}\boldsymbol{P}_k^{u}$.
4.Time update step $\boldsymbol{x}_{k+1\|k} = \boldsymbol{A}\boldsymbol{x}_{k\|k} + \boldsymbol{B}\hat{\boldsymbol{u}}_k$, $\boldsymbol{P}_{k+1\|k}^{x} = [\boldsymbol{A} \quad \boldsymbol{B}]\begin{bmatrix}\boldsymbol{P}_{k\|k}^{x} & \boldsymbol{P}_k^{xu}\\ \boldsymbol{P}_k^{ux} & \boldsymbol{P}_k^{u}\end{bmatrix}\begin{bmatrix}\boldsymbol{A}^T\\ \boldsymbol{B}^T\end{bmatrix} + \boldsymbol{G}_k$.

utilize the Kalman filtering algorithm based on excitation prediction as derived in the preceding text. This enables us to obtain the system state and excitation prediction, thereby facilitating structure response reconstruction. At this juncture, the state transfer equation and observation equation can be expressed as follows:

$$\begin{cases}\boldsymbol{x}_k = \boldsymbol{A}\boldsymbol{x}_{k-1} + \boldsymbol{B}\boldsymbol{u}_{k-1} + w_{k-1}\\ \boldsymbol{y}_k^m = \boldsymbol{H}^m\boldsymbol{x}_k + \boldsymbol{D}^m\boldsymbol{u}_k + v_k\end{cases}, \tag{27}$$

where the superscript m denotes the location of the m-th measuring point. In accordance with Eq. (27), the reconstruction response at the target point can be obtained through Kalman filtering, representing the posterior value $x_{k|k}$:

$$\boldsymbol{y}_k^r = \boldsymbol{H}^r\boldsymbol{x}_{k|k} + \boldsymbol{D}^r\hat{\boldsymbol{u}}_k\,, \tag{28}$$

where the superscript r indicates the position of the reconstruction value of the target point, $\boldsymbol{y}_k^r$ is the response value of the reconstruction of the target point. Now, if $\boldsymbol{y}_k$ is taken as the true response value of the target point, then

$$\boldsymbol{y}_k = \boldsymbol{H}^r\boldsymbol{x}_k + \boldsymbol{D}^r\hat{\boldsymbol{u}}_k\,. \tag{29}$$

When applying this algorithm to reconstruct the dynamic response of a known structure subjected to unknown excitation, it is essential to compute the structure's model parameters as algorithm parameters. Additionally, the response data collected from finite element simulations or sensors should be inputted as observation values into the algorithm. This process enables the DRR of the structure and the prediction of the excitation. Although the measurement signals in this paper are exclusively acceleration signals, this response reconstruction method remains feasible for other measurement signals such as strain, displacement, and velocity.

3. Response Reconstruction Algorithm Flow of Continuous System in Modal Space

The natural frequency, mass-normalized natural mode shape, and damping matrix of the model are directly acquired via Patran&Nastran. Once the modal truncation number is determined, the matrix $\boldsymbol{\Phi}$, $\boldsymbol{\Lambda}$, $\boldsymbol{\Gamma}$ are calculated, and then the parameter matrix $\boldsymbol{A}_C$ and $\boldsymbol{B}_C$ for the structural dynamic response method is constructed. Discretizing it using the time interval Δt, we derive the state transition matrix $\boldsymbol{A}$

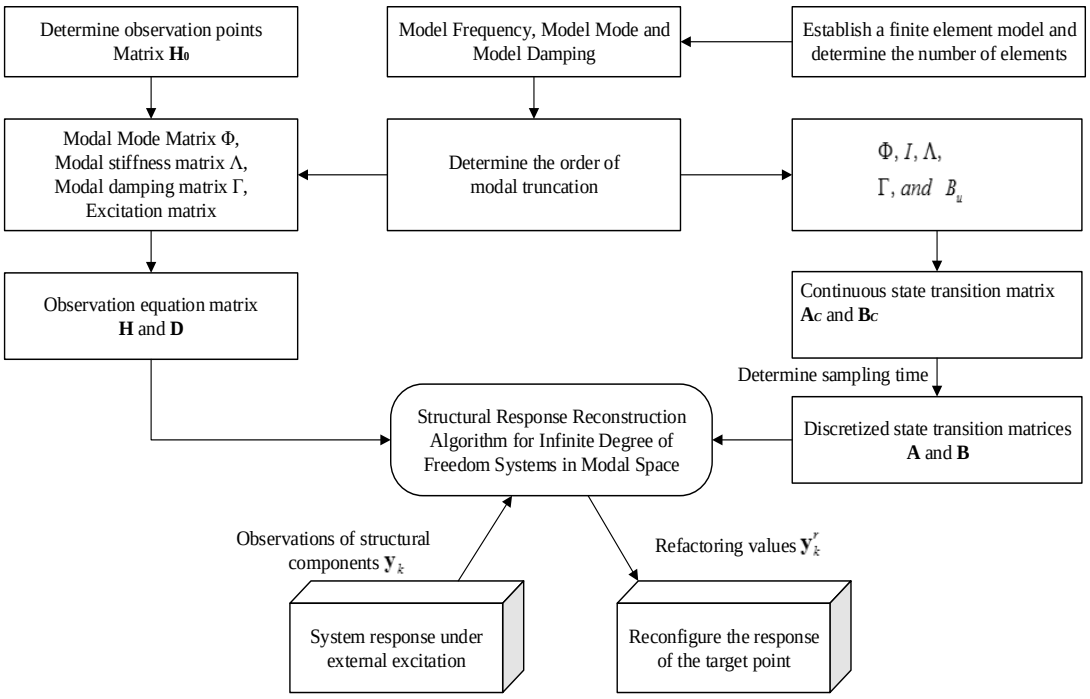

Fig. 2 Flow chart of response reconstruction method for continuous system in modal space

and excitation influence matrix $\boldsymbol{B}$. The estimation of the external excitation of the system $\hat{\boldsymbol{u}}_k$ is acquired through the excitation identification step. Simultaneously, the state estimation $\boldsymbol{x}_{k|k}$ is obtained through the measurement update step and the time update step. Leveraging the partially observed values y_k of the system response under external excitation, the response information $\boldsymbol{y}_k^r$ at the target point can be reconstructed. Fig. 2 shows the flow chart of response reconstruction method for continuous system in modal space.

4. Simulation Example

The simply supported beam model depicted in Fig. 1 has dimensions of 1 m in length, 0.05 m in width, and 0.005 m in thickness. It possesses a modulus of elasticity of 206 GPa, a density of 7900 kg/m³, and a Poisson's ratio of 0.3. A dynamic load f is applied to the beam. Following the DRR method proposed in this paper for continuous system, the dynamic response of the target point is reconstructed using response information from a finite number of points. Simultaneously, the dynamic load applied to the structure is identified and compared with the actual structural dynamic response and load to verify the feasibility and accuracy of this DRR method for a continuous structure.

4.1. Algorithm accuracy evaluation method

The peak relative error approach (*PREA*), signal to noise ratio (*SNR*) and angle cosine method (*ACM*) are used to evaluate the accuracy of load identification in this paper. We assume that the theoretically response signal is represented by $\boldsymbol{X}(i)$, while the reconstructed value is represented by $\boldsymbol{Y}(i)$.

1. *PREA*

$$PREA(\boldsymbol{X},\boldsymbol{Y}) = \frac{|max\boldsymbol{Y}(i) - max\boldsymbol{X}(i)|}{max\boldsymbol{X}(i)} \times 100\% . \quad (30)$$

PREA is used to evaluate the amplitude error between the identified value or reconstructed value and the theoretical value.

2. *SNR*

$$SNR(\boldsymbol{X},\boldsymbol{Y}) = 10log_{10}\left\{\frac{\sum_{i=1}^{n}\boldsymbol{X}(i)^2}{\sum_{i=1}^{n}\left[\boldsymbol{X}(i)-\boldsymbol{Y}(i)\right]^2}\right\}, \quad (31)$$

n is the number of samples taken within time t. The closer the recognition value or reconstruction value $\boldsymbol{Y}(i)$ is to the theoretical value $\boldsymbol{X}(i)$, the larger the *SNR*.

3. *ACM*

$$ACM(\boldsymbol{X},\boldsymbol{Y}) = cos\,\theta = \frac{\sum_{i=1}^{n}\boldsymbol{X}(i)\boldsymbol{Y}(i)}{\sqrt{\sum_{i=1}^{n}\boldsymbol{X}^2(i)\sum_{i=1}^{n}\boldsymbol{Y}^2(i)}} . \quad (32)$$

The maximum value of $ACM(X,Y)$ is 1, and the cl oser the value is to 1, the closer the recognition value or rec onstruction value signal is to the theoretical value.

4.2. Case 1: Response reconstruction under impact excitation considering modal parameter error and Gaussian white noise

For the simply supported beam model in Fig. 1, the dynamic load is assumed to be an impact load and a half sine wave within a short duration, specifically from 0.1 s to 0.110 s, while the load remains 0 at other times.

Discretize the simply supported beam model uniformly into 50 elements. Impact load $f = sin(2\pi\times50\times t)$ acting on node 21. The system begins in a zero initial state. Patran software package is utilized for modeling the simply supported beam, while Nastran software package is employed for transient dynamics analysis. The acceleration response is computed with a sampling rate of 1024, a sampling time of 5 seconds.

Taking into account actual operating conditions and modal parameter errors, as well as introducing Gaussian white noise. Assuming the observation noise follows a Gaussian distribution with a mean of 0 and a standard deviation of 10^{-3}, and incorporating a 5% modal parameter error. According to the algorithm, Fig. 3 presents a partial enlarged view of the comparison results between the load identified in the excitation identification step and the actual value at the moment of force application. Similarly, Fig. 4 illustrates the comparison between the acceleration response

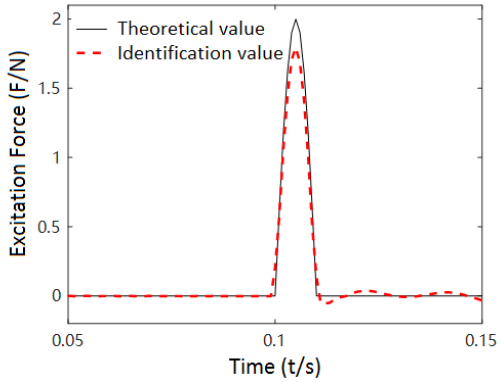

Fig. 3 Partial magnification of identification results for impact excitation with 5% modal noise error and Gaussian white noise

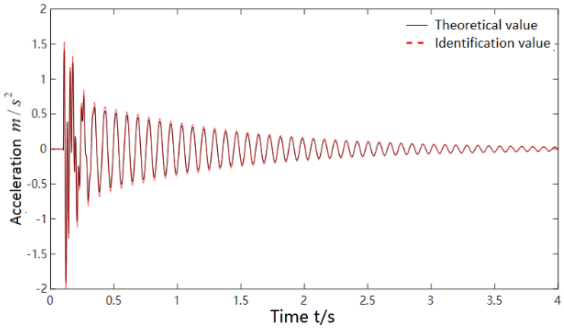

Fig. 4 Reconstruction results of acceleration response of target node with 5% modal noise error and Gaussian white noise

of target node reconstructed by the algorithm and the theoretical value. Table 2 provides the data results, which represent the average values computed from multiple data sets.

Table 2
Reconstruction error results under impact excitation with 5% modal noise and Gaussian white noise

Error evaluation method	*PREA*, %	*SNR*, dB	*ACM*
Load identification	8.33%	16.5666	0.8826
Response reconstruction	7.06%	47.2440	0.9993

As observed from the charts, when Gaussian white noise and modal parameter noise are concurrently introduced, the relative error of the *PREA* remains within 10%. The *SNR* and the *ACM* have both been affected, but they are still within the acceptable error range for practical engineering applications.

4.3. Case 2: Response reconstruction under fixed frequency excitation considering modal parameter error and Gaussian white noise

Let the dynamic load f be a fixed frequency load defined as: $f(t) = sin(2\pi\times20\times t)+3\times sin(2\pi\times20\times t)$. Same as case one, Patran is utilized to simulate model for response calculation. With a sampling rate of 1024 Hz, the sampling time is set to 5 seconds, and the acceleration response is computed accordingly. By combining the calculated response data with the natural frequencies and modes obtained through finite element analysis, we construct the parameter matrix required for the algorithm to reconstruct the response. The initial state vector of the system $x_{0|0}$ is assumed to be 0.

Assuming that the observation noise follows a Gaussian distribution with a mean of 0 and a standard deviation of 0.001, and incorporating a 5% modal parameter error. Following the algorithm, Fig.5 illustrates a partial enlarged view of the comparison results between the load identified in the excitation identification step and the actual value. Similarly, Fig. 6 presents a partial enlarged view of the comparison between the acceleration response of the target node reconstructed by the algorithm and the theoretical value. Data results, representing the average values calculated from multiple data sets, are provided in Table 3.

From the results, it is apparent that when considering the actual situation and introducing Gaussian white

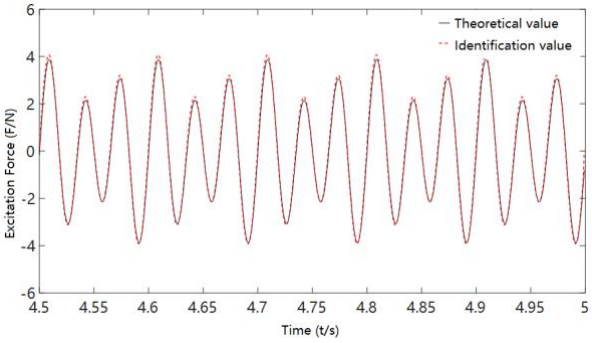

Fig. 5 Partial amplification of identification results of fixed frequency excitation with 5% modal noise error and Gaussian white noise

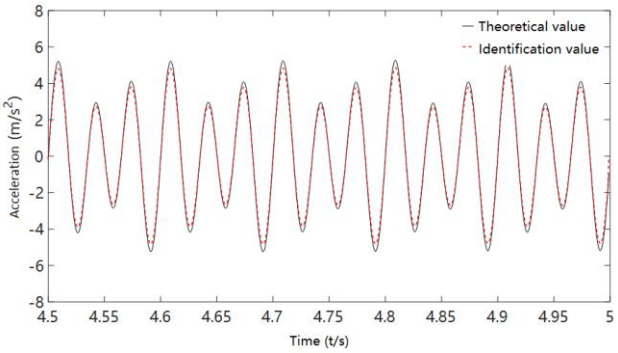

Fig. 6 Partial amplification of reconstruction results of acceleration response of target node with 5% modal noise error and Gaussian white noise

noise and modal parameter error, the *PREA* remains within 10%. Fortunately, *SNR* is relatively high, and *ACM* is close to 1, resulting in an excellent identification and reconstruction performance. This validates the feasibility and reliability of the algorithm when a fixed frequency excitation is applied to continuous system in a practical scenario.

Table 3
Reconstruction error results with 5% modal error and Gaussian white noise

Error evaluation method	*PREA*, %	*SNR*, dB	*ACM*
Load identification	5.89%	58.2600	0.9991
Response reconstruction	7.93%	51.4794	1.0000

5. Experimental Verification of Structural DRR

5.1. Structural DRR test platform and equipment

The structural DRR system is designed based on LabVIEW, encompassing both the overall scheme design and the specific software and hardware components. The correctness of the structural DRR algorithm, as well as the availability and reliability of the system, are further verified through a simply supported beam test. The test is divided into two parts:

1. Modal test of the simply supported beam structure: This part is used to obtain the natural frequency, natural mode shape, and other modal characteristics of the simply supported beam.

2. DRR test of the simply supported beam: structural DRR is completed by collecting the acceleration response of the simply supported beam. The target point response reconstruction data are obtained using the structural DRR system with limited observation points and compared with the actual measured acceleration response data of the point.

5.2. Structural DRR test

Fig. 7 shows the test site diagram, and the number of the measuring point positions on the simply supported beam. According to the test requirements, the instruments and equipment used are listed in Table 4. The test scheme for reconstructing the dynamic response of the structure under fixed frequency excitation is shown in Fig. 8.

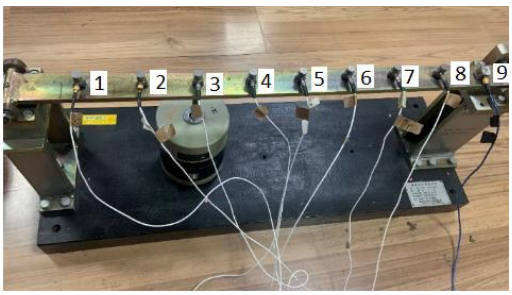

Fig. 7 Site diagram of structural DRR test

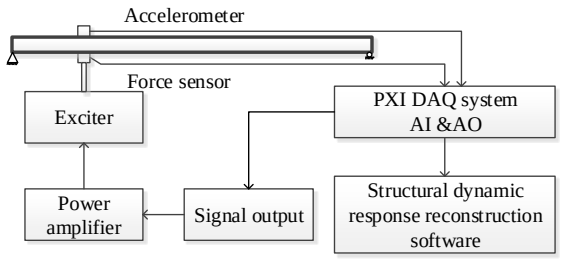

Fig. 8 Test scheme for structural DRR under fixed frequency excitation

Table 4

Test instruments and equipment for DRR testing

Equipment classification	Name	Number
Excitation equipment	PCB 086C03 hammer	1
	HEV-50 permanent magnet exciter	1
Power amplifier	HEAS-2 power amplifier	1
Dynamic signal acquisition board	NI USB 4431 acquisition card	1
	M+P AI810 acquisition card	1
Signal acquisition instrument	M+P vibmobile (up to 64 channels)	1
Sensor	PCB 356A33 unidirectional acceleration sensor	9
Software	M+P Smart Office (modal analysis)	1
	Structural dynamic response reconstruction system	1

5.3. Experimental plan for structural DRR under fixed frequency excitation

The fixed frequency excitation signal $F(t)=7\times\sin(2\pi\times50\times t)+3\times\sin(2\pi\times60\times t)$ is input.

The comparison between the load identification results and the actual excitation signal is shown in Fig. 9. The comparison between the acceleration response at measurement point of the test piece obtained through the algorithm and the actual measured response is shown in Fig. 10.

It can be observed from Fig. 9, Fig. 10 and Table 5 that the load identification and response reconstruction under fixed frequency excitation generally produce satisfactory results. The error from multi-point observation can be effectively controlled.

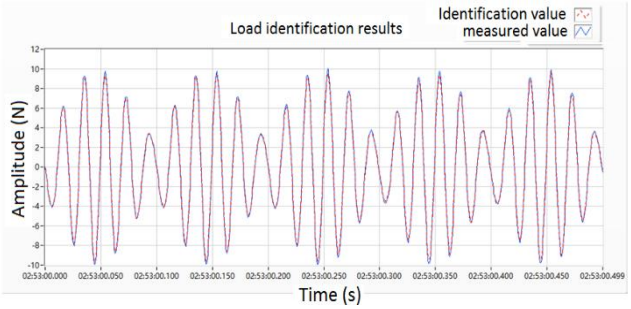

Fig. 9 Identification results of fixed frequency excitation

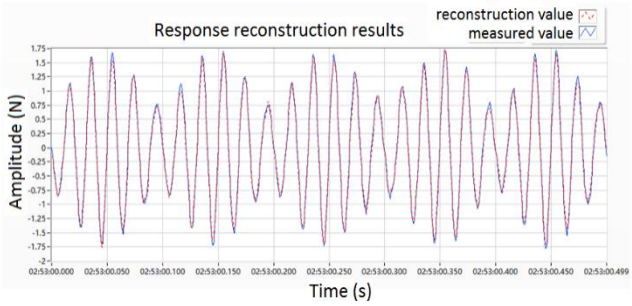

Fig. 10 Response reconstruction results of target point under fixed frequency excitation

Table 5

Reconstruction error results of fixed frequency excitation

Observation result category	Load identification		Response reconstruction	
Observation point location (test piece number)	3	2, 3, 4, 6, 8	3	2, 3, 4, 6, 8
PREA, %	2.76%	1.98%	4.46%	3.62%
SNR, dB	14.2	35.3	21.5	36.6
ACM	0.86	0.99	0.86	0.98

6. Conclusion

A response reconstruction method based on the excitation prediction Kalman filter for continuous system is established. The method can simultaneous identify the structural external excitation and reconstruct response at unmeasured positions for continuous system. Extending the algorithm from physical space to mode space for continuous system, the calculation process of the excitation prediction Kalman filter algorithm is presented. A simply supported beam system is taken as a simulation example to analyze the feasibility and reliability of load identification and response reconstruction under different external excitations, such as impact excitation and fixed frequency excitation. Various noise conditions and model errors are introduced to evaluate the noise resistance of this method. The simulation results demonstrate that the algorithm can effectively identify and reconstruct various excitations. Finally, based on the proposed structural DRR method, a test system is designed. The reconstruction test results show that *PREA* is below 5%, *SNR* is relatively high, while *ACM* is close to 1, indicating the algorithm can accurately identify the excitation under different load conditions and simultaneously reconstruct the target point response.

Acknowledgement

This research is supported by the National Natural Science Foundation of China (No.12372066 & No. U23B6009) and Foundation of National Key Laboratory of Science and Technology on Rotorcraft Aeromechanics (No.61422202105), Qing Lan Project and National Natural Science Foundation of China (No. 52171261), the Research Fund Incubation Project provided by Jinling Institute of Technology, No. jit-fhxm-201914.

References

1. **Mishra, M.; Lourenço, P. B.; Ramana, G. V.** 2022. Structural health monitoring of civil engineering structures by using the internet of things: A review, Journal of Building Engineering 48: 103954. https://doi.org/10.1016/j.jobe.2021.103954.
2. **Liu, R.; Dobriban, E.; Hou, Z.; Qian, K.** 2022. Dynamic Load Identification for Mechanical Systems: A Review, Archives of Computational Methods in Engineering 29: 831-863. https://doi.org/10.1007/s11831-021-09594-7.
3. **Wang, L.; Peng, Y.; Xie, Y.; Chen, B.; Du, Y.** 2021. A new iteration regularization method for dynamic load identification of stochastic structures, Mechanical Systems and Signal Processing 156, 107586. https://doi.org/10.1016/j.ymssp.2020.107586.
4. **Jiang, J. H.; Cui, W. X.; Chen, S.; Guo, X.; Zhao, J.** 2024. A novel dynamic load identification method based on improved basis functions and implicit Newmark-β for continuous system with unknown initial conditions, Mechanical Systems and Signal Processing 208: 110987. https://doi.org/10.1016/j.ymssp.2023.110987.
5. **Cui, W., Jiang, J.; Sun, H.; Yang, H.; Wang, X.; Wang, L.; Li, H.** 2024. Data-driven load identification method of structures with uncertain parameters. Acta Mechanica Sinica 40: 523138. https://doi.org/10.1007/s10409-023-23138-x.
6. **Yang, H.; Jiang, J.; Chen, G.; Zhao, J.** 2023. Dynamic load identification based on deep convolution neural network, Mechanical Systems and Signal Processing 185: 109757. https://doi.org/10.1016/j.ymssp.2022.109757.
7. **Li, Y.; Luo, Y. Z.; Wan, H. P.; Yun, C. B.; Shen, Y. B.** 2019. Identification of earthquake ground motion based on limited acceleration measurements of structure using Kalman filtering technique, Structural Control and Health Monitoring, 27: e2464. https://doi.org/10.1002/stc.2464.
8. **Naets, F.; Cuadrado, J.; Desmet, W.** 2015. Stable force identification in structural dynamics using Kalman filtering and dummy-measurements, Mechanical Systems and Signal Processing 50-51: 235-248. https://doi.org/10.1016/j.ymssp.2014.05.042.
9. **Aucejo, M.; De Smet, O.; Deü, J. F.** 2019. Practical issues on the applicability Kalman filtering for reconstructing mechanical sources in structural dynamics, Journal of Sound and Vibration 442: 45-70. https://doi.org/10.1016/j.jsv.2018.10.060.
10. **Maes, K.; Gillijns, S.; Lombaert, G.** 2018. A smoothing algorithm for joint input-state estimation in structural dynamics, Mechanical Systems and Signal Processing 98: 292-309. https://doi.org/10.1016/j.ymssp.2017.04.047.
11. **Huang, J. S.; Li, X. Z.; Zhang, F. B.; Lei, Y.** 2021. Identification of joint structural state and earthquake input based on a generalized Kalman filter with unknown input, Mechanical Systems and Signal Processing 151: 107362. https://doi.org/10.1016/j.ymssp.2020.107362.
12. **Álvarez-Briceño, R.; De Oliveira, L. P. R.** 2020. Combining strain and acceleration measurements for random force estimation via Kalman filtering on a cantilevered structure, Journal of Sound and Vibration 469: 15112. https://doi.org/10.1016/j.jsv.2019.115112.
13. **Hassanabadi, M. E.; Liu, Z. H.; Azam, S. E.; Dias-da-Costa, D.;** 2023. A linear Bayesian filter for input and state estimation of structural systems, Computer-Aided Civil and Infrastructure Engineering 38(13): 1749-1766. https://doi.org/10.1111/mice.12973.
14. **Tang, H.; Jiang, J.; Mohamed, M. S.; Zhang, F.; Wang, X.** 2022. Dynamic Load Identification for Structures with Unknown Parameters, Symmetry 14: 2449. https://doi.org/10.3390/sym14112449.
15. **Zhou, S.; Ward, H.** 2016. Structural Dynamics (English Version). Beijing: Beijing Institute of Technology Press.
16. **Chen, J.; Li, J.; Yang, S., Deng, F.** 2017. Weighted Optimization-Based Distributed Kalman Filter for Nonlinear Target Tracking in Collaborative Sensor Networks, in IEEE Transactions on Cybernetics 47(11): 3892-3905. https://doi.org/10.1109/TCYB.2016.2587723.

H. Li, J. Jiang, M. S. Mohamed

STUDY ON SIMULTANEOUS IDENTIFICATION OF EXTERNAL EXCIATION AND RESPONSE RECONSTRUCTION FOR CONTINUOUS SYSTEM

S u m m a r y

This paper proposes a novel dynamic response reconstruction method based on the Kalman filter which can simultaneously identify external excitation and reconstruct dynamic responses at unmeasured positions. The weighted least squares method determines the load weighting matrix for excitation identification, while minimum variance unbiased estimation determines the Kalman filter gain. The excitation prediction Kalman filter is constructed through time, excitation, and measurement updates. Subsequently, the response at the target point is reconstructed using the state vector, observation matrix, and excitation influence matrix obtained through the excitation prediction Kalman filter algorithm. An algorithm for reconstructing responses in continuous system using the excitation prediction Kalman filtering algorithm in modal space is derived. The proposed structural DRR method evaluates response reconstruction and load identification performance under various load types and errors through simulation examples. Finally, a test system for structural DRR on simply supported beams is constructed and tested. Results demonstrate accurate excitation identification under different load conditions and simultaneous reconstruction of target point responses, verifying the feasibility and reliability of the method.

Keywords: structural response reconstruction, excitation identification, Kalman filter, excitation identification Kalman filter, continuous system.

Received September 28, 2024
Accepted February 21, 2025